ELECTROMAGNETIC STUDY OF THE ITER THERMAL SHIELD

ABSTRACT

The electromagnetic (EM) loads along with seismic events and both thermal and imposed displacements are the most critical design loads for the Thermal Shield (TS) system of the International Thermonuclear Experimental Reactor (ITER). The paper is focused on the numeric approach and results of a detailed analysis of EM loads applied to the TS system during various scenarios of plasma behavior.

Keywords: thermal shield, tokamak, ITER, electromagnetic loads

I. INTRODUCTION

The thermal shield system of ITER is aimed at limiting heat loads due to heat thermal conduction and radiation on the surfaces of tokamak components operated at 4.5K. The thermal shield is designed as an actively cooled reflector between all warm (the room temperature and above) and cold (superconducting magnet structures at the temperature of liquid helium) components of the tokamak.

The thermal shield system consists of four sub-systems: a vacuum vessel thermal shield (VVTS), a cryostat thermal shield (CTS), a transition thermal shield (TTS) and a support thermal shield (STS).

VVTS, shown in Fig.1a, surrounds the hot vacuum vessel (VV) and VV ports and follows the complex VV configuration.

CTS covers the room temperature cryostat surface, while TTS bridges the space between VVTS and CTS. CTS is formed with 4 parts: CTS upper head, CTS upper cylindrical part, CTS lower cylindrical part and CTS floor. TTS for the Upper and Equatorial ports consists of the front, upper and side panels. For the CTS/TTS structure two design options were suggested: (1) a set of panels and (2) alternative, so-called self-standing closed structure. Both design options have been studied to assess their shielding capability. The main drawbacks of the panel design are complicated mounting and a high heat flux through the panel joints. The panel and alternative (self-standing) design options are presented in Fig.1b and Fig.2a respectively.

STS installed around the machine gravity support consists of the front and rear panels. STS configuration is shown in Fig.2b.

The detailed electromagnetic analysis has been carried out to predict EM loads on the thermal shield. The analysis is based on a 3D finite element (FE) representation of the thermal shield components using a thin shell approximation. The VVTS was

modeled as a single-layer shell. The CTS/TTS/STS structures were modeled with a set of 3D single-layer plates with reinforcement ribs for the panel design option.

The analysis has been performed with the use of a 3D FE code TYPHOON [1] developed at the Efremov Institute. TYPHOON allows a transient electromagnetic analysis using an FE representation of thin shell structures in an integral formulation to model arbitrary conducting walls of complex geometry.

II CALCULATION MODEL

VVTS was simulated separately from the remaining thermal shield due to accuracy requirements and extensive computational efforts involved.

For the same reason, the CTS/TTS/STS structures were divided into three separate models: CTS/TTS, CTS/TTS/STS, and the alternative self-standing CTS/TTS. Due to the symmetry, the calculation model was reduced to a 20-degree sector. The effect of eddy currents induced in VV dominates mutual induction of the panels. This allowed CTS/TTS/STS to be described by a combination of 2 sub-models: CTS/TTS sector #1 (Fig.1b) and CTS/TTS/STS sector #2 (Fig.2b) to simplify simulation and reduce a runtime.

Three resulting FE models have been developed to analyze the two CTS/TTS design options:

1) Cryostat thermal shield / transition thermal shield (CTS/TTS) (Fig. 1b);
2) Alternative cryostat thermal shield / transition thermal shield (CTS/TTS) (Fig.2a);
3) Cryostat thermal shield / transition thermal shield / support thermal shield (CTS/TTS/STS) (Fig.2b);

The Vacuum Vessel Thermal Shield (VVTS) shown in Fig.1a was modeled separately via thin shells.

VVTS is designed as a set of panels without electric contact. Each panel consists of a 35mm thick joint and two inner steel plates, 10 mm and 5 mm thick. A panel was modeled by a shell, which consists of two portions: inner and outer, as shown in Fig. 3. The outer shell simulates the joint. To imply the resistivity, the effective thickness was taken as 35mm for the outer portion of shell and 15mm for the inner portion.

Resistivity is dictated by the material properties and temperature of the conductor. At an operating temperature of 80K VVTS made of steel 304L has a resistivity of **$5.44 \cdot 10^{-7}$ Ohm·m**. For CTS/TTS and CTS/TTS/STS the resistivity was assumed constant and taken as **$5.6 \cdot 10^{-7}$ Ohm·m**. The thicknesses of the models components varied from **6mm** to **50mm** to reflect the realistic design.

Beside the single layer thermal shield and the double-walled vacuum vessel the calculation model includes the plasma, the system of toroidal field (TF) and poloidal field (PF) coils to take into consideration the ripple effect.

An important point in the model development is a topological analysis of an FE mesh. To provide adequate modelling in a thin shell formulation the first Kirchhoff law should be satisfied for furcated multi-connected conducting shells. The computational region is decomposed into simply connected domains separated with conventional sections and then reconstructed so that to produce a system of ordinary differential equations in terms of an electric vector potential. In the thin shell approximation the electric vector potential has a single component to express the eddy current density [2, 3, 4]. This allows solving a high-dimensionality problem with a dense matrix.

In the study the global Cartesian coordinate system (X,Y,Z) was used with the origin at the center of the ITER machine.

VV geometry and location remain invariable for all calculation models.

III. MODELLING OF PLASMA DISRUPTION

Variations of the full plasma toroidal current, shape and position were modeled by a current density waveforms variable in the cells of the fixed FE mesh covering the VV cross-section. The model took into account evolutions of current waveforms for all PF coils and the central solenoid (CS).

Geometrical data for the TF and PF coils were taken from [5]. The TF coil ampere-turns of 9.128MA·t were taken such that toroidal field, $B_\phi(r_0)$=5.3T at the major plasma radius r_0=6.2m. PF coils current evolutions were applied in accordance with [6, 7].

The toroidal magnetic flux generated by the plasma was simulated via a virtual toroidal solenoid located in the middle of the VV. The solenoid was assumed to generate a toroidal magnetic flux as a sum of a pure diamagnetic flux and a pure paramagnetic flux. The diamagnetic flux decays to zero at the end of the thermal quench, while the paramagnetic flux disappears at the end of the plasma current quench. Three reference scenarios of the plasma disruption were selected for the analysis of CTS/TTS/STS: slow downward vertical plasma displacement event (VDE) with Halo current [7], fast downward VDE with Halo current [7], and central disruption (CD27ms) [6].

For the reference model of the VVTS the following scenarios of plasma disruption were analyzed: Central disruption (CD27ms) [6], Central disruption (CD54ms) [6], Fast upward VDE with Halo current [7], Fast downward VDE with Halo current [7], Slow upward VDE with Halo current [7], Slow downward VDE with Halo current [7] and Toroidal coil fast discharge (TFCFD) [8].

Central disruption starts at **10ms**. Thermal quench ends at **11ms** and current quench ends at **38.5ms**.

At the Fast downward VDE, the plasma starts moving at **18ms**, thermal quench develops at **411ms** and lasts till **414ms**. The current quench is initiated at **414ms** and ends at **441ms**. The Halo current reaches its maximum of **4.91MA** at **426ms**.

At the Slow downward VDE, the plasma displacement starts at **18ms**, thermal quench occurs from **411ms** to **414ms**. The current quench starts at **414ms** and ends at **633ms**. The Halo current peaks to **6.86MA** at **513ms**.

The Halo current was pre-determined through its inlet and outlet areas. For the downward VDE the inlet area was taken in the region of the triangular frame of blanket module #1 and the outlet area in the region of the triangular frame of blanket module #17.

For the upward VDE the inlet area was taken at blanket module #8 and the outlet area at blanket module #6.

In accordance with the task definition [6], the Halo currents were assumed to have a small effect and could be neglected for the central disruption (CD27ms and CD54ms) scenarios.

IV SOLUTION SUPERPOSITION ALGORITHM

To reduce computational efforts, two different transient electromagnetic processes were simulated separately: (1) a process associated with halo currents and a variable toroidal magnetic flux generated by the plasma; and (2) a process initiated by variations of the toroidal plasma current and the PF coil currents. Obtained EM loads were then automatically superimposed with the use of a specific algorithm to produce the final results.

The superposition algorithm takes into consideration an interaction between fields and induced eddy currents for both independent numerical solutions. The total surface force density $\vec{f}_{tot}$, for each triangle finite element is found as:

$$\vec{f}_{tot} = k \cdot \vec{f}_1 + \vec{f}_2 + \left[\vec{j}_1 \times \vec{B}_2\right] + \left[\vec{j}_2 \times \vec{B}_1\right],$$

where:

- $\vec{j}_1$ is the surface current density vector produced by variations of the toroidal magnetic flux and Halo currents,
- $\vec{j}_2$ is the surface current density vector produced by variations of the toroidal plasma current and PF coil currents,
- $\vec{B}_1$ is the average field per finite element associated with variations of the toroidal magnetic flux and Halo currents;
- $\vec{B}_2$ is the average field per finite element associated with variations of the toroidal plasma current and PF coil currents;
- $\vec{B}_{ext}$ is the average field per finite element due to the toroidal plasma currents and PF and TF coil currents;
- $\vec{f}_1 = \left[\vec{j}_1 \times \left(\vec{B}_1 + \vec{B}_{ext}\right)\right]$ is the surface force density vector produced by variations of the toroidal magnetic flux and Halo currents, $\vec{f}_1$ is constant within the finite element;
- $\vec{f}_2 = \left[\vec{j}_2 \times \left(\vec{B}_2 + \vec{B}_{ext}\right)\right]$ is the surface force density vector produced by variations of the toroidal plasma current and PF coil currents, $\vec{f}_2$ is constant within the finite element;
- k is the toroidal peaking factor (taken as 1.05, 1.07, 1.27 for different scenarios of plasma disruption).

V RESULTS

The electromagnetic loads on the thermal shield have been calculated for all specified regimes. The most dangerous scenario of plasma disruption was determined for each thermal shield component by the following analysis of distributed EM loads.

Tables 1-3 summarize maximum values of total EM loads on a 20-degree TS sector for slow downward VDE, fast downward VDE and CD 27ms. The worst loading conditions are predicted for the CD27ms scenario for both CTS/TTS design options (see Tables 1-3).

The highest EM pressure of **7.42kPa** occurs at 110ms in the upper part of the front TTS panel surrounding the VV equatorial port extension (see Fig. 4). At the same time the tangential surface force density reaches **7.128kPa** in upper right and lower left corners of the front TTS panel near the VV equatorial port and on the bottom TTS panel close to the VV upper port if viewed from the center of the machine (See Fig. 5). In the same locations the surface force density tangential component is expected to peak up to **7.196kPa** at 121ms.

Peak EM loads on CTS/TTS/STS are anticipated at the upper edge of the STS lower panel at 684ms of the slow downward VDE.

The fast CD27ms produces the maximum EM pressure of **0.94MPa** at the joints of the VVTS inner part at time of **27.5ms** (see Fig. 6).

The dominant component of the total ponderomotive force applied to VVTS is the toroidal force. It is acting on a 20-degree VVTS sector and reaches **–48.8kN** at 27.5ms during the fast CD27ms (Fig. 7). The vertical moment acting on the 20°-VVTS sector has a peak of **-284kN·m** at **486ms** at the fast downward VDE (see Fig. 8). Thus, the maximum total vertical moment acting on the whole VVTS (18 sectors) is estimated as:

(–284kN·m)·18 = –5.11MN·m.

It should be noted that the EM loads on CTS/TTS due to variations of Halo current and the toroidal magnetic flux are negligible in comparison with the EM loads associated with the toroidal plasma current. A possible reason is that the field produced by the poloidal current and the Halo current on VV decays rapidly outward the VV. The

CTS/TTS/STS structure is so distant from VV that the influence of the poloidal eddy current and the Halo current can be ignored.

VI CONCLUSIONS

An effective numeric technique has been developed to estimate EM loads on the ITER Thermal Shield. The study has utilized 3D FE models. The simulations performed for a wide range of operating modes allow one to predict the most dangerous conditions when a peak surface density of the normal ponderomotive force would occur. Critical time points have been determined for all TS components. The CD27ms is expected to produce most severe load on the CTS/TTS structure, both for the panel and self-standing designs. The most loaded condition for CTS/TTS/STS is the slow downward VDE. The most critical EM loads on VVTS are reached at different scenarios of plasma discharge, i.e. toroidal force and EM pressure - at CD27ms, vertical torque moment – at fast downward VDE.

The distributed EM loads obtained from this analysis have been transferred into equivalent forces concentrated at the nodes of the reference FE mesh. For the distributed force density $\vec{f}$ this procedure practically implies integration over all space

$$\int_{V_e} N_i \ \vec{f}\, dV \ .$$

Here N_i is the shape function, V_e is the element volume,

The resulting nodal loads have been used as inputs for a subsequent structural analysis. To transform distributed loads into their nodal equivalents a code NFORCE [9] has been applied. NFORCE is applicable for most popular types of 2D and 3D FE representations and capable of producing output data in different formats including the ANSYS format.

The estimates of EM loads are of primary importance in selecting the design of thermal shield panels, supports, and joints and dictate the design concept of the thermal shield.

An overall reduction in size of the ITER machine has drawn attention back to the concept of the self-standing thermal shield. The detailed investigation of expected EM loads followed by a mechanical study confirms the advantages of this design.

The EM analysis performed has driven the conceptual design of the ITER thermal shield [10]. The results of the analysis will be included in the FDR/DDD 2003-2004.

References

1. A.V. Belov, N.I. Doinikov, A.E. Duke, et al., “Transient electromagnetic analysis in tokamaks using TYPHOON code”, Fusion Engineering and Design, **31**, pp.167-180, (1996).
2. Albanese R., Rubinacci G., “Solution of three dimensional eddy current problems by integral and differential methods”, IEEE Trans. on Magn., MAG 24, № 1, pp. 98-101, 1988.
3. Belov A.V., Doinikov N.I., Duke A.E. et al., “TYPHOON code for 3-D eddy currents simulation in conducting thin shells”, EPAC 94, London, 27 June – 1 July 1994, Proc. FOURTH Europ. Particle Accel. Conf., v. 2, pp.1224-1226.
4. Kameari A., “Transient Eddy Current Analysis on Thin Conductors with Arbitrary Connection and Shapes”, J. Of Comp. Physics, **42**, # 1, pp.124-140, (1981).
5. NAKA JWS, ITER EDA Joint Central Team, Superconducting Coils & Structures Division, “Basic Design Package for Analysis”, March 6, 2000.
6. M.Verrecchia, “FEAT type I and type II plasma disruption simulation”, ITER Memo No.G 73 MD 27 00-03-06 W 0.1, March 6, 2000.
7. M.Verrecchia, “FEAT category III fast/slow downward/upward VDE simulation”, ITER Memo No.G 73 MD 34 00-04-19 W 0.1, April 19, 2000.
8. B. Bareyt, JCT Plasma & Field Control Division, “Assessment of the TF coil discharge parameters and passive structure electro-mechanical stresses during a fast discharge”, Naka Joint Work Site, Issue 3, April 2000.
9. A. Alekseev, A. Arneman, A. Belov et al., “On the Calculation of Concentrated Loads at Finite-Element Mesh Nodes as Equivalents of a Given Spatial Distribution of Volume Force Density”, Plasma Devices and Operations,**10**(4), pp.269-284 (2002).

10. ITER Technical Basis, ITER EDA Documentation series #24, IAEA, Vienna, 2002

FIGURE CAPTIONS

Table I: Maximum EM loads and torque moments acting on 1/18 of TS at slow downward VDE.

	Maximum total EM loads (global coordinate system)			**Maximum surface force density**		**Maximum total EM torque moments** (global coordinate system)		
	radial	**toroidal**	**vertical**	**normal**	**tangential**	**radial**	**toroidal**	**vertical**
	F_x (kN)	**F_y (kN)**	**F_z (kN)**	**f_{nor} (kPa)**	**f_{tan} (kPa)**	**M_x (kN·m)**	**M_y (kN·m)**	**M_z (kN·m)**
PANEL CTS/TTS	**-5.61 (570ms)**	**0.092 (498ms)**	**-0.977 (609ms)**	**5.117 (546ms)**	**5.36 (549ms)**	**-0.185 (522ms)**	**2.3 (675ms)**	**1.34 (495ms)**
CTS/TTS/STS	**-1.49 (681ms)**	**-0.82 (690ms)**	**1.34 (678ms)**	**5.64 (684ms)**	**4.27 (684ms)**	**-4.85 (684ms)**	**-6.0 (651ms)**	**-7.09 (690ms)**
SELF-STANDING CTS/TTS	**-39.4 (588ms)**	**-3.93 (759ms)**	**-1.95 (657ms)**	**8.71 (552ms)**	**11 (606ms)**	**-3.4 (534ms)**	**-53.4 (516ms)**	**-46.8 (759ms)**
VVTS	**24.2 (555ms)**	**44.6 (450ms)**	**-28.8 (489ms)**	**401 (579ms)**	**51.9 (447ms)**	**-148 (660ms)**	**-84.8 (660ms)**	**-237 (621ms)**

Table II: Maximum EM loads and torque moments acting on 1/18 of TS at <u>fast downward VDE.</u>

	Maximum total EM loads (global coordinate system)			**Maximum surface force density**		**Maximum total EM torque moments** (global coordinate system)		
	radial	**toroidal**	**vertical**	**normal**	**tangential**	**radial**	**toroidal**	**vertical**
	F_x (kN)	**F_y (kN)**	**F_z (kN)**	**f_{nor} (kPa)**	**f_{tan} (kPa)**	**M_x (kN·m)**	**M_y (kN·m)**	**M_z (kN·m)**
PANEL CTS/TTS	**-6.87 (522ms)**	**0.103 (471ms)**	**-1.25 (510ms)**	**6.29 (498ms)**	**6.45 (513ms)**	**-0.174 (528ms)**	**2.09 (522ms)**	**1.55 (477ms)**
CTS/TTS/STS	**-1.37 (561ms)**	**-0.758 (582ms)**	**1.3 (552ms)**	**5.38 (567ms)**	**4.14 (561ms)**	**-4.5 (573ms)**	**-7.13 (513ms)**	**-6.53 (576ms)**
SELF-STANDING CTS/TTS	**-48.4 (531ms)**	**-4.44 (633ms)**	**-2.25 (513ms)**	**10.6 (507ms)**	**13.6 (534ms)**	**-3.87 (507ms)**	**-41.2 (438ms)**	**-52.7 (639ms)**
VVTS	**11.8 (471ms)**	**39 (428ms)**	**-16.5 (439ms)**	**553 (438ms)**	**56.2 (430ms)**	**-181 (510ms)**	**-55.7 (510ms)**	**-284 (486ms)**

Table III: Maximum EM loads and torque moments acting on 1/18 of TS at CD27ms.

	Maximum total EM loads (global coordinate system)			**Maximum surface force density**		**Maximum total EM torque moments** (global coordinate system)		
	radial	**toroidal**	**vertical**	**normal**	**tangential**	**radial**	**toroidal**	**vertical**
	F_x (kN)	**F_y (kN)**	**F_z (kN)**	**f_{nor} (kPa)**	**f_{tan} (kPa)**	**M_x (kN·m)**	**M_y (kN·m)**	**M_z (kN·m)**
PANEL CTS/TTS	**-7.78 (132ms)**	**0.058 (82.5ms)**	**-1.32 (132ms)**	**7.42 (110ms)**	**7.196 (121ms)**	**-0.206 (160ms)**	**2.63 (46.2ms)**	**1.09 (99ms)**
CTS/TTS/STS	**-1.22 (154ms)**	**-0.665 (165ms)**	**1.16 (132ms)**	**4.73 (160ms)**	**3.64 (154ms)**	**-3.96 (170ms)**	**-6.88 (93.5ms)**	**-5.74 (170ms)**
SELF-STANDING CTS/TTS	**-53.4 (138ms)**	**-4.35 (160ms)**	**-1.36 (47.3ms)**	**11.6 (126ms)**	**14.4 (132ms)**	**-3.6 (143ms)**	**-68.4 (138ms)**	**-51.1 (160ms)**
VVTS	**10.3 (33ms)**	**-48.8 (27.5ms)**	**6.49 (110ms)**	**940 (27.5ms)**	**94.8 (33ms)**	**-203 (11ms)**	**-69.5 (116ms)**	**-175 (60.5ms)**

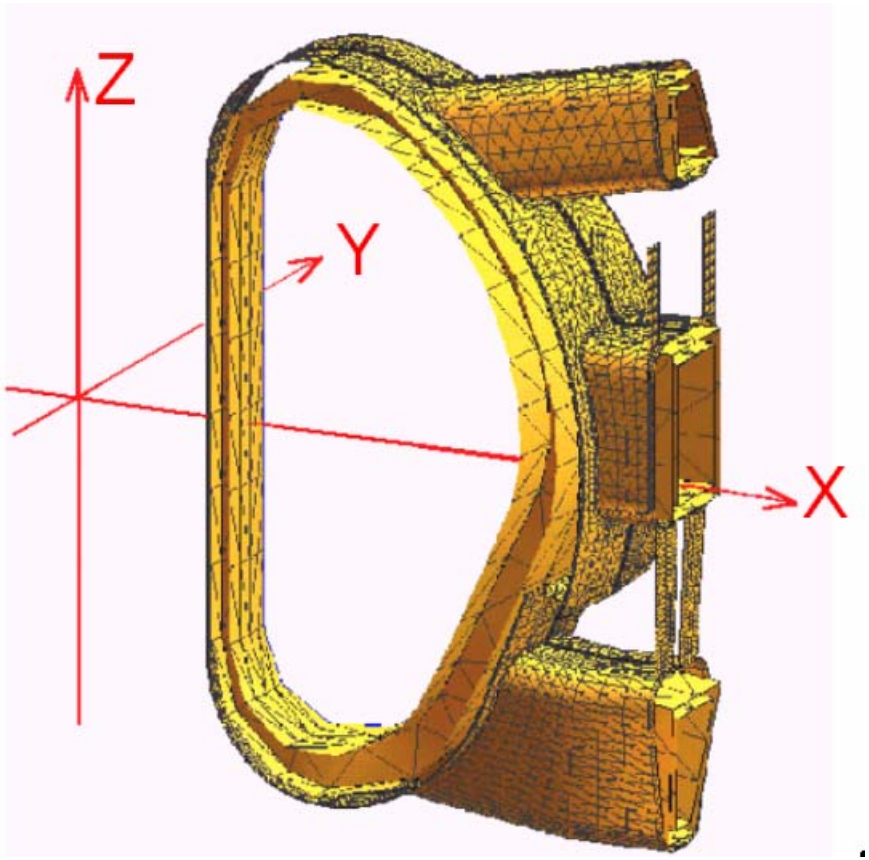

a

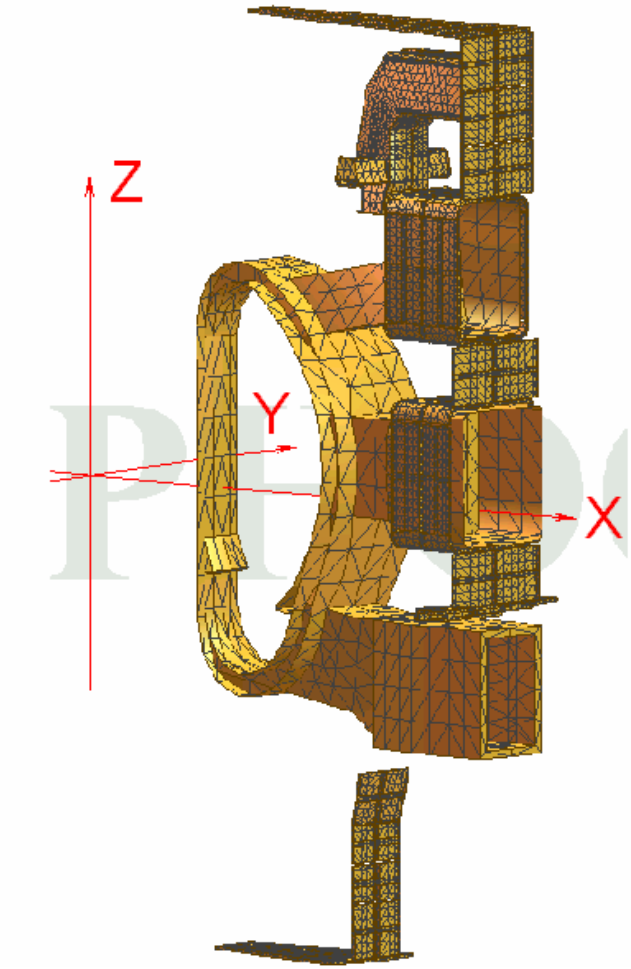

b

Figure 1: Calculation models

a) VVTS (1/18 of thermal shield)
b) CTS/TTS (1/18 of thermal shield). Panel design.

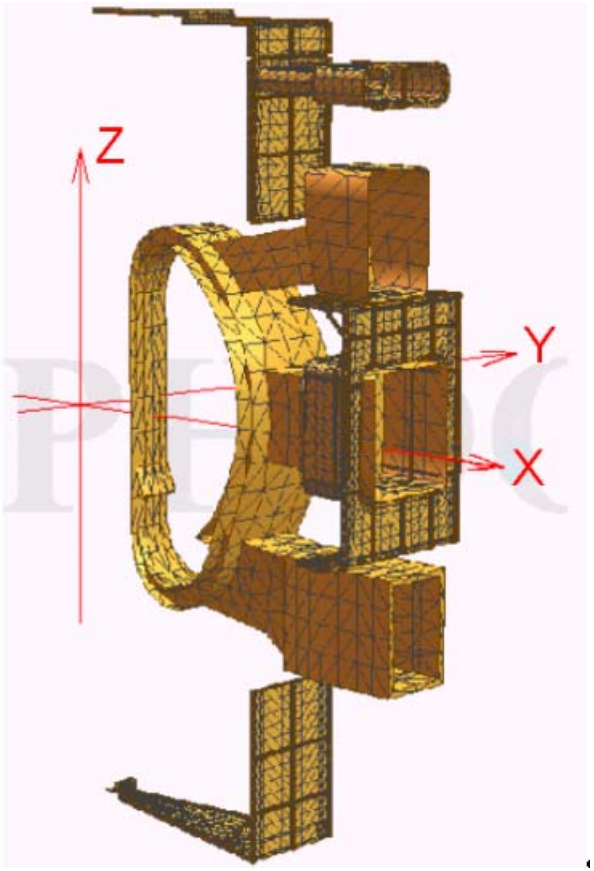

a

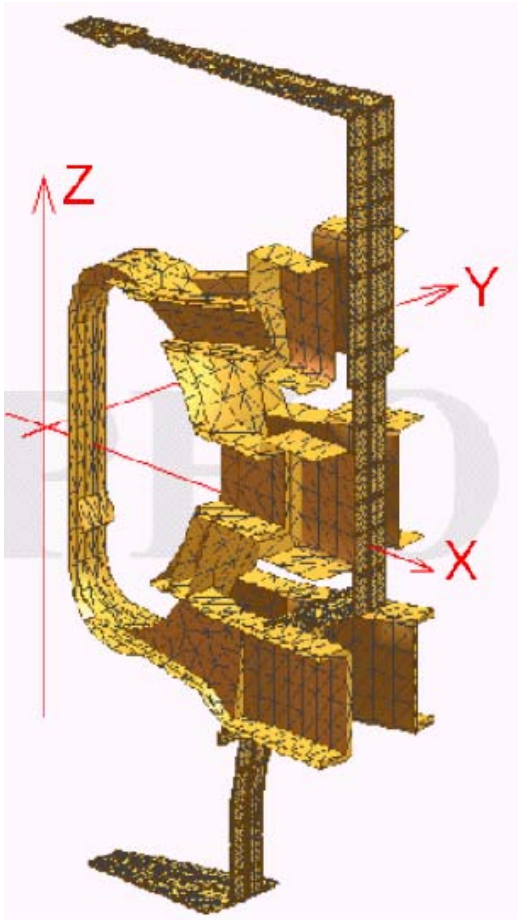

b

Figure 2: Calculation models

a) CTS/TTS (1/18 of thermal shield). Alternative (self-standing) design
b) CTS/TTS/STS (1/18 of thermal shield).

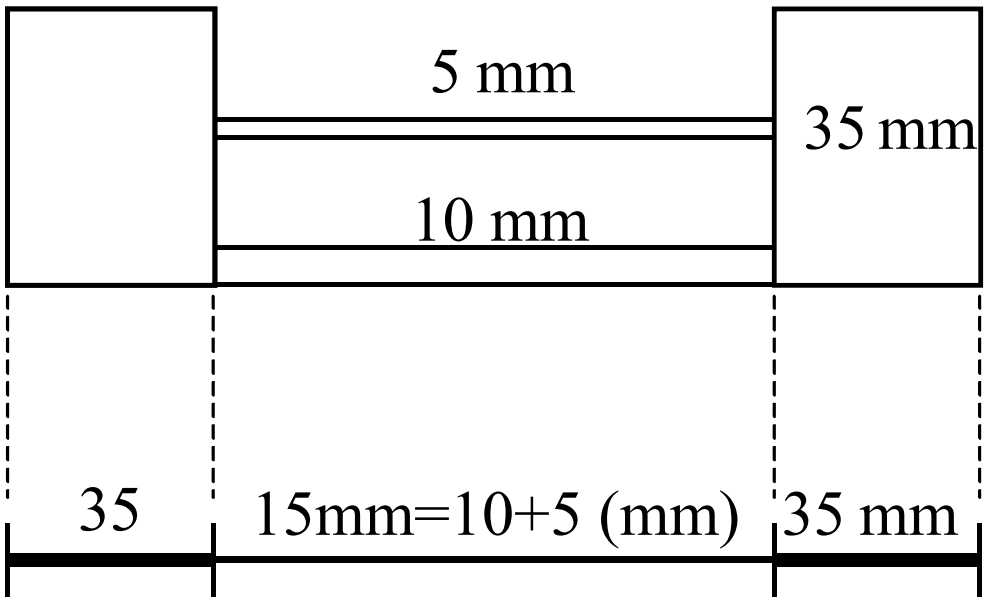

Figure 3: VVTS panel middle cross-section and panel model shell.
Real solid construction of VVTS, including 35mm joints and two panels with different thicknesses.
The mathematical model of VVTS represents real construction via thin shells

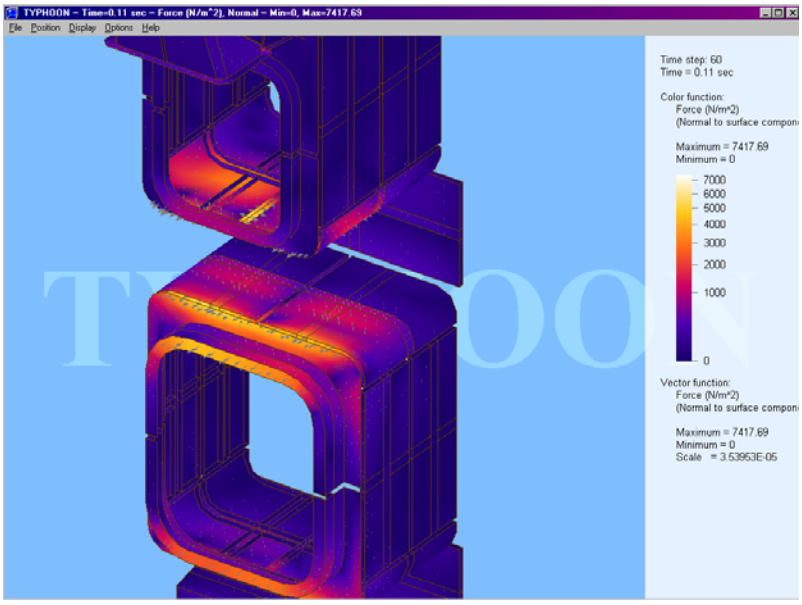

Figure 4: Distribution of normal surface force density on CTS/TTS at 110ms. Zoom in (CD 27ms).

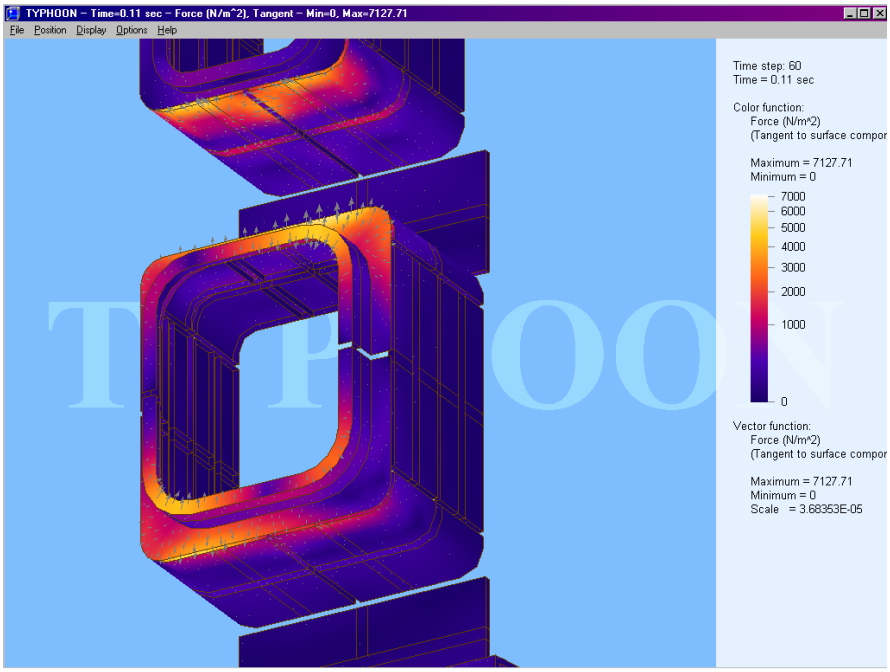

Figure 5: Distribution of tangential surface force density on CTS/TTS at 110ms. Zoom in (CD 27ms).

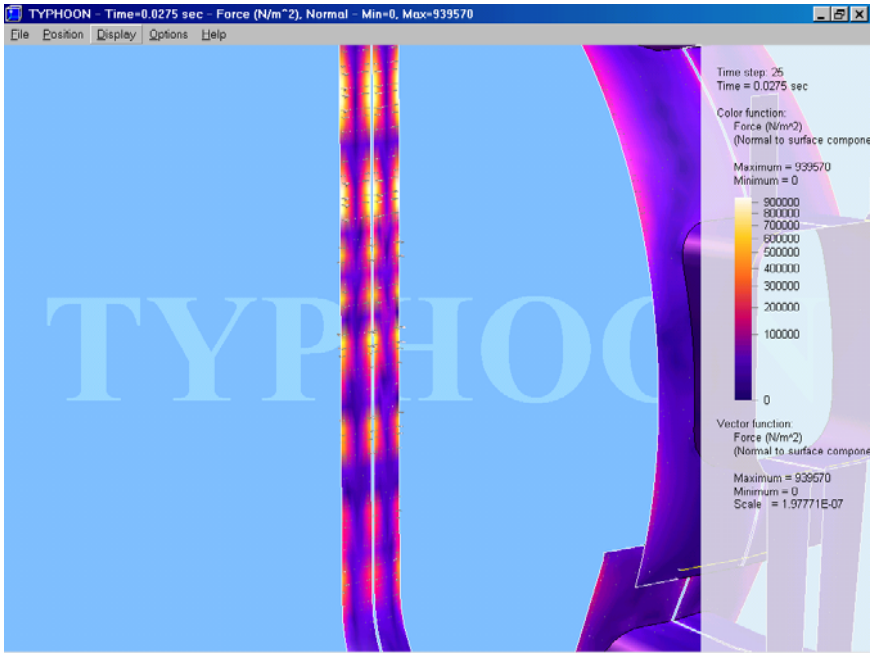

Figure 6: Inner part of VVTS. Distribution of normal component of surface force density during CD27ms at 27.5ms.

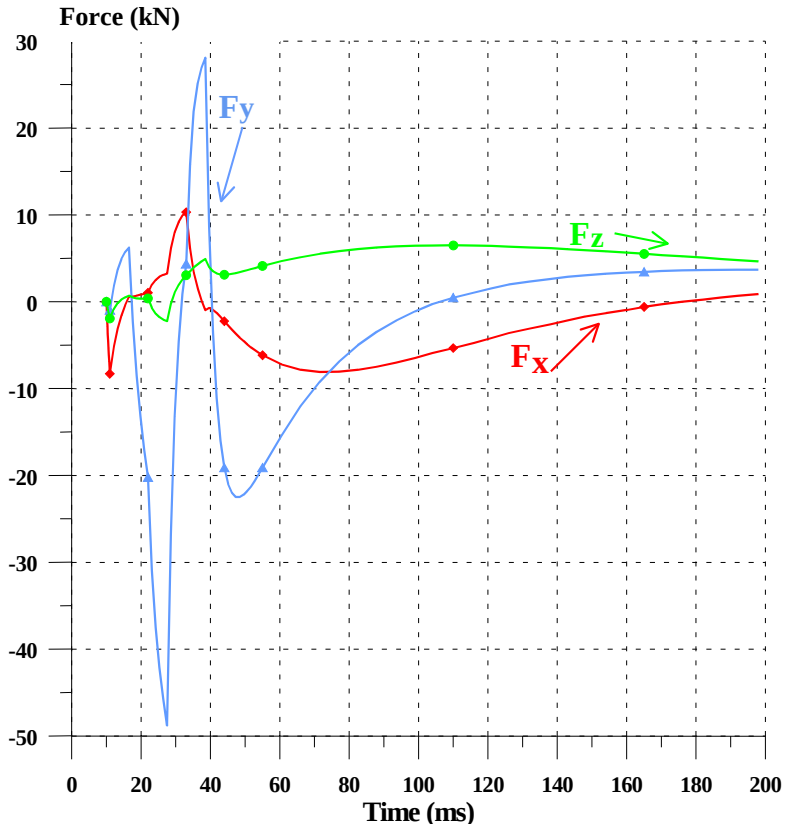

Figure 7: Evolutions of total horizontal and vertical forces acting on a 1/18 of VVTS during fast CD27ms. The global Cartesian coordinate system is shown in Figure 1.

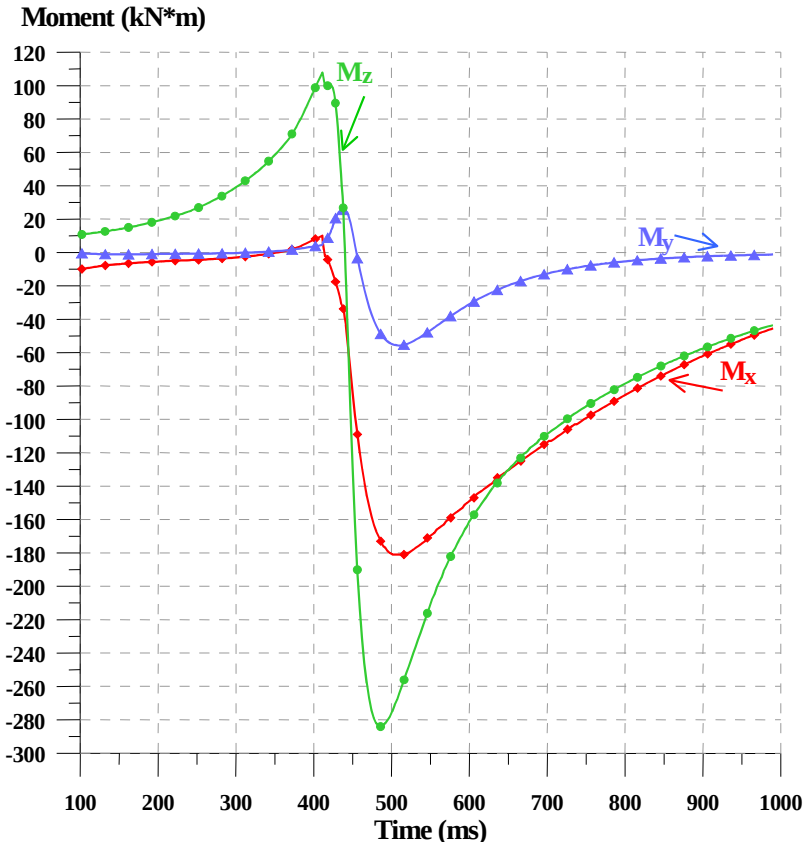

Figure 8: Evolutions of total horizontal and vertical torque moments acting on a 1/18 of VVTS during fast downward VDE. The global Cartesian coordinate system is shown in Figure 1.